Electronics and Communications in Japan, Vol. 96, No. 10, 2013
Translated from Denki Gakkai Ronbunshi, Vol. 132-C, No. 5, May 2012, pp. 721–729

Stabilizing Predictive Visual Feedback Control via Image Space Navigation Function

TOSHIYUKI MURAO,[1] HIROYUKI KAWAI,[2] and MASAYUKI FUJITA[3]
[1]Advanced Institute of Industrial Technology, Japan
[2]Kanazawa Institute of Technology, Japan
[3]Tokyo Institute of Technology, Japan

SUMMARY

This paper investigates stabilizing receding horizon control via an image space navigation function for three-dimensional (3D) visual feedback systems. First, we describe the representation of a relative pose and a camera model. Next, a visual motion error system which can handle time-varying desired motion is constructed. Then, visual motion observer-based stabilizing receding horizon control for 3D visual feedback systems is proposed. Moreover, a path planner appropriate for the visual motion error system is designed through an image space navigation function to keep all features in the camera field of view. The main contribution of this paper is to show that the path planner which always remains in the camera field of view during servoing is designed for position-based visual feedback receding horizon control based on optimal control theory. Finally, we present simulation and nonlinear experimental results in order to verify control performance with visibility maintenance of the proposed control scheme. © 2013 Wiley Periodicals, Inc. Electron Comm Jpn, 96(10): 12–21, 2013; Published online in Wiley Online Library (wileyonlinelibrary.com). DOI 10.1002/ecj.11493

Key words: visual feedback control; receding horizon control; navigation function; passivity; stability.

1. Introduction

Visual feedback control is a very flexible and effective method for the autonomous performance of various tasks for robotic systems [1]. Many researchers have tackled the various problems of visual feedback control [2–4].

In particular, there has been an increase of interest in problems in which all feature points remain within the camera field of view since the work of Chaumette [5]. Navigation functions that are globally convergent potential functions are reported to yield very good results for the camera field of view problem [6–8]. Cowan and colleagues [6] proposed a visual feedback controller to bring a robot to rest at a desired configuration for the field of view problem by using navigation functions. In Ref. 7, a model-based geometric visual servoing framework capable of occlusion-free servoing through the navigation function method was presented. Chen and colleagues [8] developed an off-line path planner based on an image space navigation function with an adaptive 2.5D visual servoing controller. However, the desired control performance cannot always be guaranteed explicitly, since these useful control methods [6–8] are not based on optimization.

On the other hand, receding horizon control, also recognized as model predictive control, is a well-known control strategy in which a current control action is computed by solving a finite horizon optimal control problem on-line [9]. For visual feedback systems, a few implementations of receding horizon control have been reported. Sauvée and colleagues [10] proposed an image-based visual servoing scheme based on nonlinear model predictive control for robot systems. In Ref. 11, nonlinear model predictive control of instrument motion based on ultrasound images is investigated. Recently, the results of comparison between the two image prediction models—a nonlinear global model and a local model based on the interaction matrix—were given in Ref. 12. Although good receding horizon control approaches for the visual feedback system considering mechanical and visibility constraints are reported in Refs. 10–12, stability is not addressed. In Refs. 13 and 14, the authors proposed stabilizing receding horizon control for 3D visual feedback systems, as predictive visual feedback control. However, this position-based visual feedback control method through the nonlinear receding horizon approach can allow feature points to leave the field of view.

In this paper, we propose stabilizing receding horizon control via an image space navigation function for 3D visual feedback systems with an eye-in-hand configuration as shown in Fig. 1. First, a visual motion error system which can handle time-varying desired motion is constructed. Second, stabilizing receding horizon control for the visual motion error system using a control Lyapunov function is proposed. Then, a path planner appropriate for the visual motion error system is designed through an image space navigation function in order to keep all features within the camera field of view. Path planning on an image space could be of significant benefit when used in conjunction with the proposed position-based receding horizon control by using an error defined on a Cartesian space. Finally, the control performance with visibility maintenance of the proposed control scheme and with the previous scheme [13] is evaluated through simulation and nonlinear experimental results.

The paper is organized as follows. In Section 2, we propose stabilizing predictive visual feedback control for a time-varying desired relative pose. In Section 3, we design a path planner based on an image space navigation function. Sections 4 and 5 describe simulation and experimental results that show the advantages of the proposed control law, followed by conclusions in Section 6.

2. Stabilizing Predictive Visual Feedback Control

2.1 Vision camera model

Visual feedback systems with an eye-in-hand configuration use three coordinate frames: the world frame Σ_w, the camera frame Σ_c, and the object frame Σ_o, as in Fig. 1. Let $p_{ab} \in \mathcal{R}^3$ and $e^{\hat{\xi}\theta_{ab}} \in SO(3)$ be the position vector and the rotation matrix from a frame Σ_a to a frame Σ_b. Then, the relative pose from Σ_a to Σ_b can be represented by

$$g_{ab} = \begin{bmatrix} e^{\hat{\xi}\theta_{ab}} & p_{ab} \\ 0 & 1 \end{bmatrix} \in \mathcal{R}^{4\times 4} \tag{1}$$

where the notation "∧" denotes the skew-symmetric operator [15]. In contrast, the notation "∨" denotes the inverse operator to "∧."

The relative pose from Σ_c to Σ_o can be derived by using the composition rule for rigid body transformations [15] as follows:

$$g_{co} = g_{wc}^{-1} g_{wo} \tag{2}$$

Differentiating Eq. (2) with respect to time, the body velocity of the relative pose g_{co} can be written as follows (see Ref. 16):

$$V_{co}^b = -\mathrm{Ad}_{(g_{co}^{-1})} V_{wc}^b + V_{wo}^b \tag{3}$$

where $V_{wc}^b \in \mathcal{R}^6$ and $V_{wo}^b \in \mathcal{R}^6$ are the body velocities of the camera and the target object relative to Σ_w, respectively. The notation $\mathrm{Ad}_{(g_{ab})}$ represents the adjoint transformation associated with g_{ab} [15].

The relative pose $g_{co} = (p_{co}, e^{\hat{\xi}\theta_{co}})$ cannot be immediately obtained in the visual feedback system, because the target object velocity V_{wo}^b is unknown and furthermore cannot be measured directly. To control the camera using visual information provided by a computer vision system, we use the pinhole camera model with a perspective projection as shown in Fig. 2. Here, we consider four feature points on the rigid target object in this paper. Let λ be the focal length, α_x and α_y be the scaling factors along the x and y axes (in pixels/meter), and $p_{oi} \in \mathcal{R}^3$ and $p_{coi} \in \mathcal{R}^3$ be the position vectors of the target object's i-th feature point

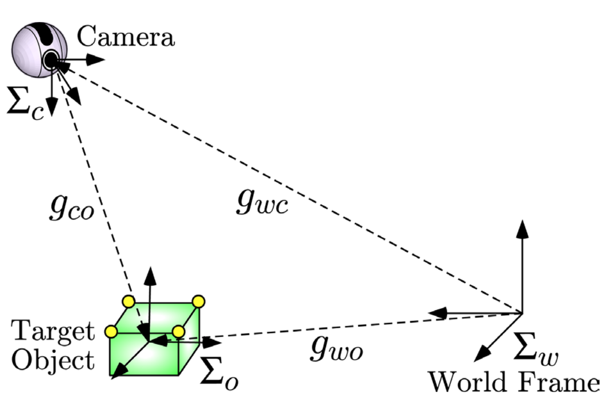

Fig. 1. Visual feedback system with an eye-in-hand configuration. [Color figure can be viewed in the online issue, which is available at wileyonlinelibrary.com.]

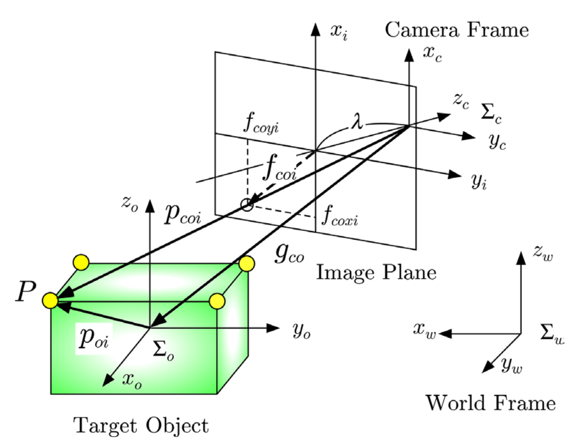

Fig. 2. Pinhole camera model. [Color figure can be viewed in the online issue, which is available at wileyonlinelibrary.com.]

relative to Σ_o and Σ_c, respectively. Using a transformation of coordinates, we have $p_{coi} = g_{co}p_{oi}$, where p_{coi} and p_{oi} should be regarded, with a slight abuse of notation, as $[p_{coi}^T 1]^T$ and $[p_{oi}^T 1]^T$ via the well-known homogeneous coordinate representation in robotics, respectively (see, e.g., Ref. 15).

The perspective projection of the i-th feature point onto the image plane gives us the image plane coordinate $f_{coi} := [f_{coxi} f_{coyi}]^T \in \mathcal{R}^2$ as

$$f_{coi} = \frac{1}{z_{coi}} \begin{bmatrix} \lambda\alpha_x & 0 \\ 0 & \lambda\alpha_y \end{bmatrix} \begin{bmatrix} x_{coi} \\ y_{coi} \end{bmatrix} \tag{4}$$

where $p_{coi} = [x_{coi}\ y_{coi}\ z_{coi}]^T$. It is straightforward to extend this model to four image points by simply stacking the vectors of the image plane coordinate, that is, $f_{co} = [f_{co1}^T \ldots f_{co4}^T]^T \in \mathcal{R}^8$. Hereafter, f_{ab} means $f(g_{ab})$ for simplicity.

2.2 Visual motion error system

The objective of position-based visual feedback control is, in general, to bring the actual relative pose g_{co} to the desired one g_{cd}. Although we handle the time-varying desired pose g_{cd}, the final desired one is assumed to be constant from the practical point of view in this paper. The visual feedback control task requires information on the relative pose g_{co}. Since the only measurable information is the image features f_{co} in the visual feedback system, we consider the following visual motion observer based on Eq. (3) in order to estimate the relative pose g_{co} from the image features f_{co}:

$$\bar{V}_{co}^b = -\mathrm{Ad}_{(\bar{g}_{co}^{-1})} V_{wc}^b + u_e \tag{5}$$

where $\bar{g}_{co}$ and $\bar{V}_{co}^b \in \mathcal{R}^6$ are the estimated values of the relative pose and body velocity, respectively. The new input $u_e \in \mathcal{R}^6$ is to be determined in order to drive the estimated values $\bar{g}_{co}$ and $\bar{V}_{co}^b$ to their actual values.

Here we define the pose control error g_{ec} and the estimation error g_{ee} as follows:

$$g_{ec} := g_{cd}^{-1} g_{co} \tag{6}$$

$$g_{ee} := \bar{g}_{co}^{-1} g_{co} \tag{7}$$

Using the notations $r_{ei} := \mathrm{sk}(e^{\hat{\xi}\theta_{ei}})^\vee \in \mathcal{R}^3$ and $\mathrm{sk}(e^{\hat{\xi}\theta_{ei}}) := 1/2(e^{\hat{\xi}\theta_{ei}} - e^{-\hat{\xi}\theta_{ei}}) \in \mathcal{R}^{3\times 3}$, we next define the vectors of the pose control error and the estimation error as $e_c := [p_{ec}^T\ r_{ec}^T]^T \in \mathcal{R}^6$ and $e_e := [p_{ee}^T\ r_{ee}^T]^T \in \mathcal{R}^6$, respectively. The estimation error vector e_e can be obtained from the image features f_{co} and the estimated value of the relative pose $\bar{g}_{co}$ (i.e., the measurement and the estimate) as follows:

$$e_e = J_e^\dagger(\bar{g}_{co})(f_{co} - \bar{f}_{co}) \tag{8}$$

where $\bar{f}_{co} \in \mathcal{R}^8$ is the estimated value of the image features and $J(\bar{g}_{co}) \in \mathcal{R}^{8\times 6}$ is an image Jacobian-like matrix [16]. The pose control error vector e_c can also be calculated by using the desired relative pose g_{cd} and the estimation error vector e_e [14].

Differentiating Eqs. (6) and (7) with respect to time, we construct the visual motion observer-based pose control error system (which we call the visual motion error system) as follows:

$$\begin{bmatrix} V_{ec}^b \\ V_{ee}^b \end{bmatrix} = \begin{bmatrix} -\mathrm{Ad}_{(g_{ec}^{-1})} & 0 \\ 0 & -\mathrm{Ad}_{(g_{ee}^{-1})} \end{bmatrix} u + \begin{bmatrix} I \\ I \end{bmatrix} V_{wo}^b \tag{9}$$

where

$$u := [u_c^T\ u_e^T], \quad u_c := \mathrm{Ad}_{(g_{cd}^{-1})} V_{wc}^b + V_{cd}^b \tag{10}$$

and $V_{cd}^b \in \mathcal{R}^6$ is the body velocity of the desired relative pose g_{cd}. Although the visual motion error system (9) in this paper has the same form as in Refs. 13 and 14, the input u is different in the two systems. Let us define the error vector of the visual motion error system as $x := [e_c^T\ e_e^T]^T$, which consists of the pose control error vector e_c and the estimation error vector e_e. It should be noted that if the vectors of the pose control error and the estimation error are equal to zero, then the actual relative pose g_{co} tends to the desired one g_{cd} when $x \to 0$. In the case that the target object is static (that is, $V_{wo}^b = 0$), the visual motion error system (9) is passive from the input u to the output x. The passivity property can be proved by using the following positive definite function:

$$V(x) = E(g_{ec}) + E(g_{ee}) \tag{11}$$

where $E(g_{ei}) := 1/2\|p_{ei}\|^2 + \phi(e^{\hat{\xi}\theta_{ei}}) \in \mathcal{R}$ and $\phi(e^{\hat{\xi}\theta_{ei}}) := 1/2\,\mathrm{tr}(I - e^{\hat{\xi}\theta_{ei}}) \in \mathcal{R}$ is the error function of the rotation matrix [17].

2.3 Stabilizing predictive visual feedback control

In this subsection, the finite horizon optimal control problem (FHOCP) for visual motion error system (9) is considered. The FHOCP for system (9) at time t consists of the minimization with respect to the input $u(\tau, x(\tau))$, $\tau \in [t, t+T]$, of the following cost function:

$$J(x_0, u, T) = \int_t^{t+T} l(x(\tau), u(\tau))d\tau + F(x(t+T)) \tag{12}$$

$$l(x(t), u(t)) = E_{qc}(g_{ec}(t)) + E_{qe}(g_{ee}(t)) + u^T(t)R(t)u(t) \tag{13}$$

$$F(x) = \rho V(x)$$

$$q_{pi}(t) \geq 0,\ q_{ri}(t) \geq 0,\ R(t) > 0,\ \rho > 0 \tag{14}$$

where $R(t)$ is a positive diagonal matrix, and $E_{qi}(g_{ei}(t)) := q_{pi}(t)\|p_{ei}(t)\|^2 + q_{ri}(t)\phi(e^{\hat{\xi}\theta_{ei}(t)})$, with the state $x(t) = x_0$. For a given initial condition x_0, we denote this solution of the FHOCP as $u^*(\tau, x(\tau))$, $\tau \in [t, t+T]$. In receding horizon control, at each sampling time δ, the resulting feedback control at state x_0 is obtained by solving the FHOCP and setting

$$u^{RH} := u^*(\delta, x_0) \tag{15}$$

Assuming that the target object is static, we have the following theorem concerning the convergence of the stabilizing receding horizon control for the visual feedback system.

Theorem 1 Consider cost function (12)–(14) for visual motion error system (9). Suppose that $V_{wo}^b = 0$, $|\theta_{ec}| \leq \pi/2$, $|\theta_{ee}| \leq \pi/2$, and $\rho^2 I \geq 4QR$; then the receding horizon control for the visual motion error system is asymptotically stabilizing.

Theorem 1 guarantees the stability of receding horizon control by using the fact that the energy function $\rho V(x)$ of the visual motion error system (9) can be regarded as a control Lyapunov function in the case of $\rho^2 I \geq 4QR$. One of the contributions of this paper is that the proposed control law can be applied to the time-varying desired relative pose $g_{cd}(t)$, similar to the case of a constant one [13, 14]. Since the stabilizing receding horizon control design is based on optimal control theory, the control performance should be improved under the condition of adequate gain assignment in the cost function.

3. Image Space Navigation Function-Based Path Planning

3.1 Design of desired body velocity

The inherent problem of position-based visual feedback control using only an error defined on a Cartesian space has been stated, namely, that it is difficult to assure that the target object will always remain in the camera field of view during servoing [5]. Because the proposed stabilizing receding horizon control in the previous section is a position-based method, it may leave the camera field of view. In this section, a path planner appropriate for the visual motion error system is designed through an image space navigation function to guarantee that all features will remain in the camera field of view. The control objective in this paper is stated as follows:

Control Objective: The vision camera follows the target object, that is, the relative pose $g_{co}(t)$ coincides with the time-varying desired one $g_{cd}(t)$ which is generated to keep all features within the camera field of view, and which converges to the final desired one g_{cd_f}.

From the proposed stabilizing receding horizon control law (15) and the input to the visual motion error system (10), the input to the vision camera is designed as follows:

$$V_{wc}^b = \mathrm{Ad}_{(g_{cd})}\left(u_c^{RH} - V_{cd}^b\right) \tag{16}$$

where $u^{RH} = [(u_c^{RH})^T\ (u_e^{RH})^T]^T$. The desired relative pose g_{cd} can be obtained by solving the equation

$$\dot{g}_{cd} = g_{cd}\hat{V}_{cd}^b \tag{17}$$

Hence, the vision camera input V_{wc}^b needs only the body velocity V_{cd}^b.

Here we introduce the navigation function-based method as a technique for constructing artificial potential fields in order to design V_{cd}^b which can achieve the control objective. First, we define the desired image feature vector and the final one as $f_{cd} := f(g_{cd})$ and $f_{cd_f} := f(g_{cd_f})$, respectively. The navigation function used in this paper is defined as follows:

Definition 1 [7, 8] Let D be a space where all feature points of the target object remain visible, and let f_{cd_f} be in the interior of D. A smooth Morse function $\varphi(f_{cd}) : D \to [0, 1]$ is a navigation function if

1. a unique minimum exists at f_{cd_f};
2. it is admissible on D, that is, uniformly maximal on the boundary of D.

To develop the desired body velocity V_{cd}^b, we derive a relationship between f_{cd} defined on the image space and V_{cd}^b defined on the Cartesian space. Using the desired feature point $p_{cdi} = [x_{cdi}\ y_{cdi}\ z_{cdi}]^T$, the desired image features can be obtained as follows:

$$f_{cdi} = \frac{1}{z_{cdi}}\begin{bmatrix} \lambda\alpha_x & 0 \\ 0 & \lambda\alpha_y \end{bmatrix}\begin{bmatrix} x_{cdi} \\ y_{cdi} \end{bmatrix} \tag{18}$$

Differentiating Eq. (18), the relation between the desired image features f_{cd_i} and the desired feature point p_{cd_i} can be expressed as

$$\dot{f}_{cdi} = \begin{bmatrix} \frac{\lambda\alpha_x}{z_{cdi}} & 0 & -\frac{\lambda\alpha_x x_{cdi}}{z_{cdi}^2} \\ 0 & \frac{\lambda\alpha_y}{z_{cdi}} & -\frac{\lambda\alpha_y y_{cdi}}{z_{cdi}^2} \end{bmatrix}\dot{p}_{cdi} \tag{19}$$

Moreover, we have the following relation between the desired feature point p_{cd_i} and the body velocity V_{cd}^b through $p_{cdi} = g_{cd}p_{oi}$:

$$\dot{p}_{cdi} = e^{\hat{\xi}\theta_{cd}}\begin{bmatrix} I & -\hat{p}_{oi} \end{bmatrix}V_{cd}^b \tag{20}$$

Hence, the desired image feature vector and the desired body velocity can be related as

$$\dot{f}_{cd} = J_L(g_{cd})V_{cd}^b \tag{21}$$

where $J_L(g_{cd}) : SE(3) \to \mathcal{R}^{8\times 6}$ is defined as follows:

$$J_L(g_{cd}) := \begin{bmatrix} J_{L1}^T(g_{cd}) & J_{L2}^T(g_{cd}) & \cdots & J_{L4}^T(g_{cd}) \end{bmatrix}^T \quad (22)$$

$$J_{Li}(g_{cd}) := \begin{bmatrix} \frac{\lambda\alpha_x}{z_{cdi}} & 0 & -\frac{\lambda\alpha_x x_{cdi}}{z_{cdi}^2} \\ 0 & \frac{\lambda\alpha_y}{z_{cdi}} & -\frac{\lambda\alpha_y y_{cdi}}{z_{cdi}^2} \end{bmatrix} e^{\hat{\xi}\theta_{cd}} \begin{bmatrix} I & -\hat{p}_{oi} \end{bmatrix}$$
$$(i = 1, \cdots, 4) \quad (23)$$

Inspired by Eq. (18) and the definition of the navigation function, the desired body velocity V_{cd}^b is designed as follows:

$$V_{cd}^b = -k_{cd} J_L^\dagger(g_{cd}) \nabla\varphi(f_{cd}) \quad (24)$$

where $\nabla\varphi(f_{cd}) := (\partial\varphi(f_{cd})/\partial f_{cd})^T \in \mathcal{R}^8$ denotes the gradient vector of $\varphi(f_{cd})$ and $k_{cd} \in \mathcal{R}$ is the positive gain. The design of the image navigation function $\varphi(f_{cd})$ is stated in the Appendix.

The stabilizing predictive visual feedback control law can be applied to the system by using the desired body velocity V_{cd}^b given by Eq. (24) and the desired relative pose g_{cd} which is obtained by solving Eq. (17).

3.2 Convergence analysis for path planner

Substituting Eq. (20) into Eq. (18), we obtain for the velocity of the desired image feature vector

$$\dot{f}_{cd} = -k_{cd} J_L(g_{cd}) J_L^\dagger(g_{cd}) \nabla\varphi(f_{cd}) \quad (25)$$

Similarly to Ref. 8, it is assumed that $\nabla\varphi(f_{cd}) \notin NS(J_L^T(f_{cd}))$, where $NS(\cdot)$ denotes the null space operator. Since f_{cd} is chosen a priori via the off-line path planning routine in Eq. (25), this assumption can be satisfied.

Assuming that $\nabla\varphi(f_{cd})$ is not a member of the null space $J_L^T(f_{cd})$, the following theorem concerning the convergence of the path planner holds.

Theorem 2 Suppose that $\nabla\varphi(f_{cd}) \notin NS(J_L^T(f_{cd}))$ and the initial desired image feature vector $f_{cd}(0)$ satisfies $f_{cd}(0) \in D$. Then, the desired image feature vector (25) ensures that $f_{cd}(t) \in D$ and the desired relative pose $g_{cd}(t)$ has the asymptotically stable equilibrium point g_{cd_f}.

Proof: Consider the following positive definite function:

$$V_n(f_{cd}(t)) = \varphi(f_{cd}(t)) \quad (26)$$

Evaluating the time derivative of $V_n(f_{cd})$ along the trajectories of Eq. (25) gives

$$\begin{aligned} \dot{V}_n(f_{cd}(t)) &= (\nabla\varphi)^T \dot{f}_{cd} \\ &= -k_{cd}(\nabla\varphi)^T J_L J_L^\dagger \nabla\varphi \\ &= -k_{cd}(J_L^T\nabla\varphi)^T (J_L^T J_L)^{-1} J_L^T \nabla\varphi \\ &\le -k\|J_L^T\nabla\varphi\|^2 \end{aligned} \quad (27)$$

where we use the property $k|a|^2 \le k_{cd} a^T (J_L^T J_L)^{-1} a,\ \forall a \in \mathcal{R}^6$, and k denotes a positive constant. It is clear from Eq. (27) that $V_n(f_{cd})$ is a nonincreasing function in the sense that

$$V_n(f_{cd}(t)) \le V_n(f_{cd}(0)) \quad (28)$$

From Eqs. (26) to (28), the condition $f_{cd}(t) \in D,\ \forall t > 0$ is satisfied for any initial condition $f_{cd}(0) \in D$. By LaSalle's Theorem, it can be proved that the only invariant set that satisfies $|J_L^T(f_{cd})\nabla\varphi(f_{cd})| = 0$ is the origin. Considering the assumption $\nabla\varphi(f_{cd}) \notin NS(J_L^T(f_{cd}))$, we have shown that $|\nabla\varphi(f_{cd})| = 0$. By the argument in the Appendix, it can be shown that $f_{cd}(t) \to f_{cd_f}$. Since only one geometric solution of $g_{cd}(t)$ exists due to the fact that we set four feature points on the target object, it can be concluded that $g_{cd}(t) \to g_{cd_f}$. □

Theorem 2 guarantees the convergence of the time-varying desired image feature vector $f_{cd}(t)$ to the final one f_{cd_f}. The path planner can be designed to keep all features within the camera field of view based on the image space navigation function. A block diagram of the visual motion stabilizing receding horizon control with the image space navigation function-based path planner is shown in Fig. 3.

Although position-based control can allow feature points to leave the field of view, its principal advantages are that it is possible to describe tasks in terms of Cartesian pose, as is common in many applications, such as robotics [1], and that it does not need a desired image a priori. Thus, the proposed method which combines the position-based receding horizon control and the image-based path planner allows us to extend the technological application area. The main contribution of this paper is to present the path planner which always remains in the camera field of view during servoing, which is designed for the position-based visual feedback receding horizon control based on optimal control theory.

It is also interesting to note that the Jacobian $J_L(\cdot)$ between the image feature vector and the body velocity has exactly the same form as the Jacobian $J_e(\cdot)$ for the estimation error, which is derived by using a first Taylor expansion approximation. It leads to application to visual feedback systems with a panoramic camera using the Jacobian $J(\cdot)$ in Ref. 18.

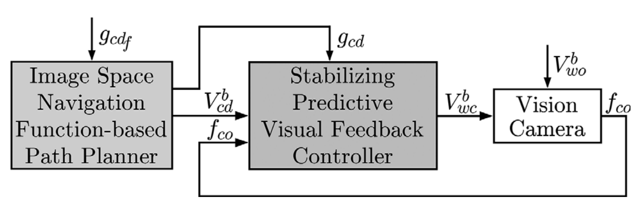

Fig. 3. Block diagram of stabilizing predictive visual feedback control with image space navigation function-based path planner.

Our previous work has proposed stabilizing receding horizon control for visual feedback systems with manipulator dynamics [13, 14]. In a similar way, our proposed approach can be applied to robot systems which must be controlled with a small sampling period.

4. Simulation Results

In this section, we present simulation results for the visual feedback control with the path planner via the image space navigation function, compared with the constant desired motion proposed in Ref. 13.

The simulation was carried out with the initial conditions $p_{co} = [0.2\ 0.2\ -1.35]^T$ m, $\xi\theta_{co} = [0\ 0\ 0]^T$ rad. The final desired relative pose was $p_{cd_f} = [-0.22\ -0.31\ -1.35]^T$ m, $\xi\theta_{cd_f} = [0\ 0\ \pi/2]^T$ rad. This condition means that the vision camera moves from end to end of the field of view diagonally with optical axis rotation. We set the maximum and minimum pixel values of the vision camera as $f_{xM} = 240$ pixels, $f_{xm} = -240$ pixels, $f_{yM} = 320$ pixels, $f_{ym} = -320$ pixels. The weights of the cost function (12)–(14) were selected as $q_{pc} = 0.003$, $q_{rc} = 0.001$, $q_{pe} = 0.0003$, $q_{re} = 0.0001$, and $R = \mathrm{diag}\{0.105, 0.105, 15, 15, 15, 0.105, 300, 300, 30, 30, 30, 300\}$ and $\rho = 1$ satisfied $\rho^2 I \geq 4QR$. To solve the real-time optimization problem, the software C/GMRES [19] was utilized. The control input with receding horizon control was updated every 2 ms and had to be calculated by the receding horizon controller within that period. The horizon was selected as $T = 0.04$ s. The parameters for the trajectory generation were selected as $k_{cd} = 6000000$, $K_s = 0.1I$, $\kappa = 2$.

The simulation results are presented in Figs. 4 to 6. In Fig. 4, the norm of the state x applying the proposed control law is shown. The asymptotic stability can be confirmed by steady-state performance. Figure 5 shows the

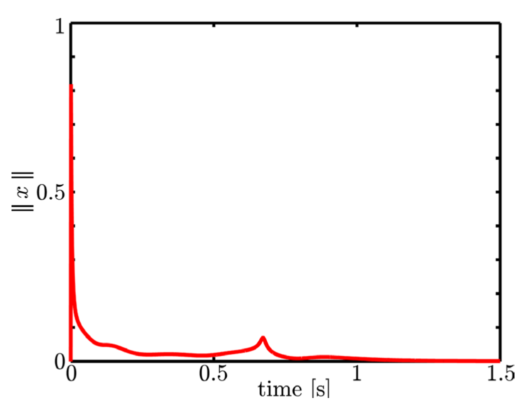

Fig. 4. Norm of the state. [Color figure can be viewed in the online issue, which is available at wileyonlinelibrary.com.]

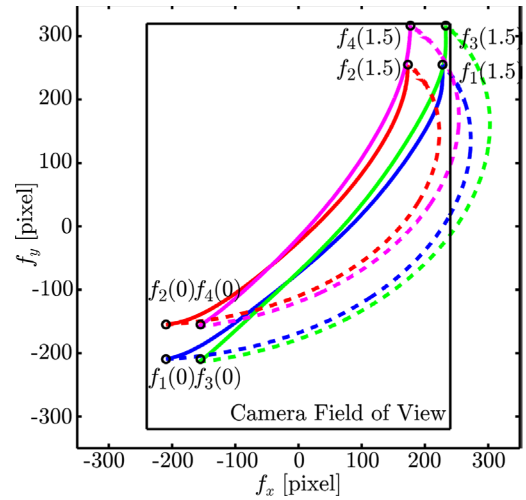

Fig. 5. Trajectory of image feature points (solid: with proposed method; dashed: with previous one [13]). [Color figure can be viewed in the online issue, which is available at wileyonlinelibrary.com.]

trajectory of the image feature points f_{co}. In Fig. 5, the solid lines denote the trajectory applying the proposed stabilizing receding horizon control with the path planner, and the dashed lines denote those for the constant desired value [13], respectively. $f_{co}(0) := [f_1^T(0)\, f_2^T(0)\, f_3^T(0)\, f_4^T(0)]^T$ and $f_{co}(1.5) := [f_1^T(1.5)\, f_2^T(1.5)\, f_3^T(1.5)\, f_4^T(1.5)]^T$ show the values of the image feature vector in the case of the initial conditions and in the case of $t = 1.5$ s, respectively. The control method must be designed so that the feature points do not leave the camera field of view, which is shown by a rectangle in Fig. 5. From Fig. 5 it is concluded that the proposed

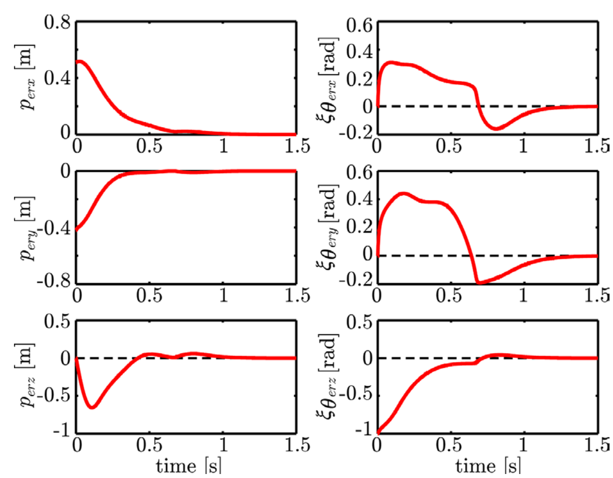

Fig. 6. Pose control error. [Color figure can be viewed in the online issue, which is available at wileyonlinelibrary.com.]

Table 1. Values of the integral cost with simulation results

Control Scheme	cost
Passivity based Control	10.3159
Receding Horizon Control ($T = 0.04$ [s])	0.5826
Receding Horizon Control ($T = 0.4$ [s])	0.5813
Receding Horizon Control ($T = 1$ [s])	0.5799

method can make the vision camera keep all feature points in the field of view. Although convergence to the desired values was also achieved by the previous method [13] in the simulation, it corresponds to failure in the actual experiment because the vision camera misses the target object.

Figure 6 shows the actual pose control error e_r, which is the error vector between the current relative pose $g_{co}(t)$ and the final desired one g_{cd_f}, instead of the time-varying desired one $g_{cd}(t)$. It can be confirmed that all errors converge to zero by steady-state performance. It should be noted that the position error with the z-axis and the rotation error with the x-axis and y-axis increases, while the others are monotonically decreasing. This means that the vision camera moves away and changes orientation once in order to keep the target object in the camera field of view. This validates one of the expected advantages of stabilizing receding horizon control with the path planner for the visual feedback system.

Next the performance for the horizon length T is compared in terms of the integral cost in Table 1. The cost is calculated by the function

$$Cost = \int_0^I l(x(\tau), u(\tau))d\tau \tag{29}$$

We set the integration interval I = 1.5 in this simulation. Since the cost of the stabilizing receding horizon method is smaller than that of the passivity-based visual feedback control method under conditions of the adequate cost function, it can be easily verified that the control performance is improved. As the horizon length increases from $T = 0.04$ s to $T = 1$ s, the cost is reduced. In the case of $T = 10$ s, the calculation cannot be completed within one sampling interval, due to limited computing power.

5. Experimental Results

In this section, we present experimental results with an omnidirectional mobile robot from Tosa Denshi, Ltd., as shown in Fig. 7. We set up a KMT-1607N (30 fps) camera on the mobile robot. The video signals were acquired by a PicPort-Stereo-H4D frame grabber board and the HALCON image processing software. The mobile robot was controlled by a digital signal processor (DSP) DS1104 (dSPACE Inc.) whose sampling time was 10 ms. The control signal was transmitted through XBees.

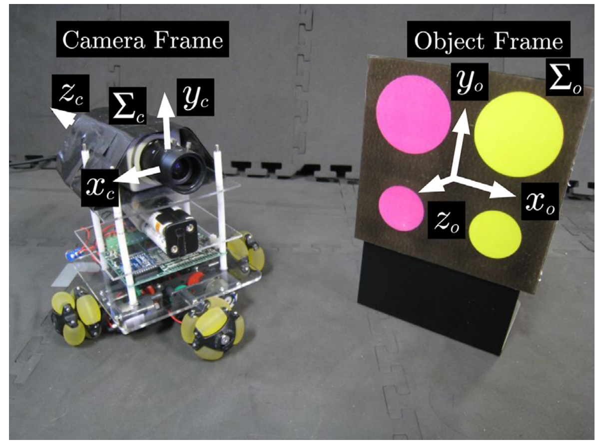

Fig. 7. Mobile robot and target object. [Color figure can be viewed in the online issue, which is available at wileyonlinelibrary.com.]

Due to environmental constraints, we performed the experimental verification with non-optical-axis rotation, but the simulation verification with optical axis rotation. The experiment was carried out with the following conditions, parameters, and weights: $p_{co} = [0.2\ 0\ {-1.3}]^T$ m, $\xi\theta_{co} = [0\ \pi/12\ 0]^T$ rad, $p_{cd_f} = [0.03\ 0\ {-0.6}]^T$ m, $\xi\theta_{cd_f} = [0\ 0\ 0]^T$ rad, $f_{xM} = 350$ pixels, $f_{xm} = -350$ pixels, $f_{yM} = 200$ pixels, $f_{ym} = -200$ pixels, $q_{pc} = 0.008$, $q_{rc} = 0.005$, $q_{pe} = 0.2$, $q_{re} = 0.15$, $R = \mathrm{diag}\{1.5, 1.5, 1.75, 0.8, 0.8, 0.8, 0.05, 0.05, 0.05, 0.06, 0.06, 0.06\}$, $\rho = 1$, $T = 0.05$ s, $k_{cd} = 140000$, $K_s = \mathrm{diag}\{0.1, 0.05, 0.1, 0.05, 0.1, 0.05, 0.1, 0.05\}$, $\kappa = 2$.

The experimental results are presented in Figs. 8 to 10. The pose control error and the estimation error are shown on the left and right sides of Fig. 8, respectively. We focus on the errors in the translation of x and z and the rotation of y, because the errors in the translation of y and the rotations of x and z are ideally zero in the defined

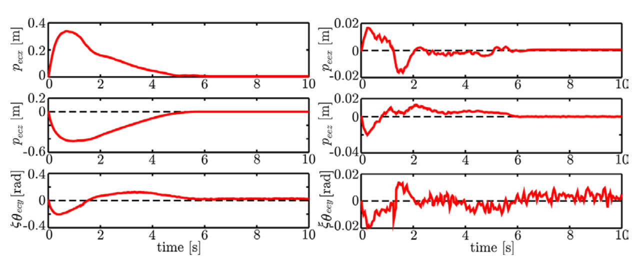

Fig. 8. Pose control error and estimation one. [Color figure can be viewed in the online issue, which is available at wileyonlinelibrary.com.]

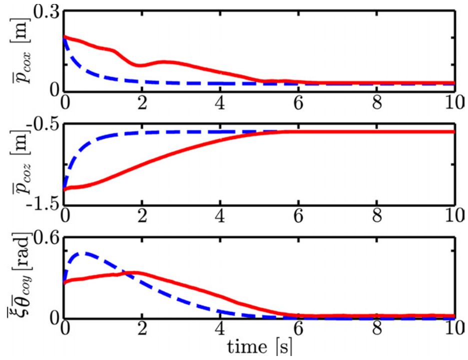

Fig. 9. Estimated relative pose. [Color figure can be viewed in the online issue, which is available at wileyonlinelibrary.com.]

coordinates in Fig. 7. Since we set the weights and gains in order not to reach the voltage limits of the mobile robot, the convergence time of the experimental results is longer than that of the simulation results. Although a slight error remains in the steady state because of image noise and the friction force with the robot, it can be confirmed that all errors converge to zero.

In Fig. 9, the solid and dashed lines respectively represent the estimated relative pose and the desired relative pose generated on the basis of the image space navigation

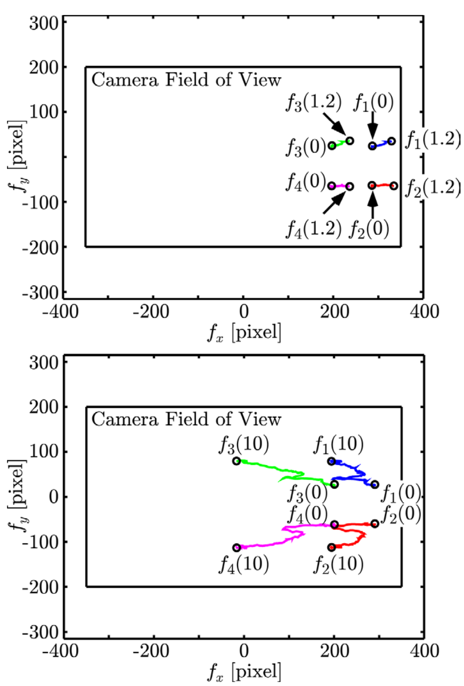

Fig. 10. Trajectory of image feature points (top: with previous method [13]; bottom: with proposed one). [Color figure can be viewed in the online issue, which is available at wileyonlinelibrary.com.]

Table 2. Values of the integral cost with experimental results

Control Scheme	cost
Passivity based Control	13.7056
Receding Horizon Control ($T = 0.01$ [s])	11.4265
Receding Horizon Control ($T = 0.05$ [s])	10.1662
Receding Horizon Control ($T = 0.5$ [s])	7.9265
Receding Horizon Control ($T = 1$ [s])	5.2540

function. It can be verified that the relative pose tracks the desired one, and that a time delay occurs. Figure 10 shows the trajectory of the image features f_{co}. In Fig. 10, the top and bottom graphs show the trajectories obtained by the previous method [13] and the proposed method, respectively. In the case of the previous method [13], the mobile robot is controlled so as to reduce the errors in the Cartesian space. However, the vision camera misses the target object at 1.2 s because the control approach is not proposed on the basis of the image space. As a result, the experiment fails under this condition. On the other hand, it can be confirmed that the vision camera moves to the desired value while keeping all feature points in the camera field of view in the case of the proposed method.

Finally, the performance with respect to the horizon length T is compared in terms of the integral cost calculated by Eq. (29) with $I = 15$ in Table 2. Similarly to the simulation results, the cost is reduced as the horizon length increases. Therefore, the validity of the stabilizing predictive visual feedback control which can keep all feature points in the camera field of view is confirmed by the experimental results.

6. Conclusions

This paper proposes stabilizing receding horizon control via an image space navigation function for 3D eye-in-hand visual feedback systems. Regarding the image space navigation function as a Lyapunov function, convergence analysis for the proposed path planner is provided. The main contribution of this paper is to show that a path planner which always remains in the camera field of view during the servoing is designed for the position-based visual feedback receding horizon control based on optimal control theory. Simulation and nonlinear experimental results are presented to verify the control performance with visibility maintenance of the proposed control scheme.

REFERENCES

1. Chaumette F, Hutchinson SA. Visual servoing and visual tracking. In Siciliano B, Khatib O (editors).

Springer handbook of robotics. Springer-Verlag; 2008. p 563–583.
2. Gans NR, Hutchinson SA. Stable visual servoing through hybrid switched-system control. IEEE Trans Robot 2007;23:530–540.
3. Lippiello V, Siciliano B, Villani L. Position-based visual servoing in industrial multirobot cells using a hybrid camera configuration. IEEE Trans Robot 2007;23:73–86.
4. Mansard N, Chaumette F. Directional redundancy for robot control. IEEE Trans Automatic Control 2009;54:1179–1192.
5. Chaumette F. Potential problems of stability and convergence in image-based and position-based visual servoing. In Kriegman DJ, Hager GD, Morse AS (editors). The confluence of vision and control. Lect Notes Control Inf Sci 1998;237:66–78.
6. Cowan NJ, Weingarten JD, Koditschek DE. Visual servoing via navigation functions. IEEE Trans Robot Automation 2002;18:521–533.
7. Cowan NJ, Chang DE. Geometric visual servoing. IEEE Trans Robot 2005;21:1128–1138.
8. Chen J, Dawson DM, Dixon WE, Chitrakaran VK. Navigation function-based visual servo control. Automatica 2007;43:1165–1177.
9. Mayne DQ, Rawlings JB, Rao CV, Scokaert POM. Constrained model predictive control: Stability and optimality. Automatica 2000;36:789–814.
10. Sauvée M, Poignet P, Dombre E, Courtial E. Image based visual servoing through nonlinear model predictive control. Proc 45th IEEE Conference on Decision and Control, p 1776–1781, 2006.
11. Sauvée M, Poignet P, Dombre E. Ultrasound image-based visual servoing of a surgical instrument through nonlinear model predictive control. Int J Robot Res 2008;27:25–40.
12. Allibert G, Courtial E, Chaumette F. Predictive control for constrained image-based visual servoing. IEEE Trans Robot 2010;26:933–939.
13. Murao T, Kawai H, Fujita M. Predictive visual feedback control with eye-in/to-hand configuration via stabilizing receding horizon approach. Proc 17th IFAC World Congress on Automatic Control, p 5341–5346, 2008.
14. Murao T, Kawai H, Fujita M. Stabilizing predictive visual feedback control for fixed camera systems. Electron Commun Jpn 2011;94:1–11.
15. Murray R, Li Z, Sastry SS. A mathematical introduction to robotic manipulation. CRC Press; 1994.
16. Fujita M, Kawai H, Spong MW. Passivity-based dynamic visual feedback control for three dimensional target tracking: Stability and L_2-gain performance analysis. IEEE Trans Control Syst Technol 2007;15:40–52.
17. Bullo F, Lewis AD. Geometric control of mechanical systems. Springer-Verlag; 2004.
18. Kawai H, Murao T, Fujita M. Passivity-based visual motion observer with panoramic camera for pose control. J Intell Robot Syst 2011;64(3–4):561–583.
19. Ohtsuka T. A continuation/GMRES method for fast computation of nonlinear receding horizon control. Automatica 2004;40:563–574.

APPENDIX

The Image Space Navigation Function

This section presents the image space navigation function $\varphi(f_{cd})$ [6, 8]. The image space navigation function is designed so that all image features remain in the visible set.

$$\eta(f_{cd}) = \mathrm{diag}\left\{\frac{2}{f_{x_M} - f_{x_m}}, \frac{2}{f_{y_M} - f_{y_m}}, \cdots \frac{2}{f_{y_M} - f_{y_m}}\right\} f_{cd} - \left[\frac{f_{x_M} + f_{x_m}}{f_{x_M} - f_{x_m}}\ \frac{f_{y_M} + f_{y_m}}{f_{y_M} - f_{y_m}}\ \cdots\ \frac{f_{y_M} + f_{y_m}}{f_{y_M} - f_{y_m}}\right]^T \tag{30}$$

$$s(\eta) = \left[\frac{\eta_1 - \eta_{f1}}{(1-\eta_1^{2\kappa})^{\frac{1}{2\kappa}}}\ \cdots\ \frac{\eta_8 - \eta_{f8}}{(1-\eta_8^{2\kappa})^{\frac{1}{2\kappa}}}\right]^T \tag{31}$$

First, we define two auxiliary functions $\eta(f_{cd}) : \mathcal{R}^8 \to [-1, 1]^8$ and $s(\eta) : [-1, 1]^8 \to \mathcal{R}^8$ as follows: where $\eta(f_{cd}) = [\eta_1(f_{cd})\ \eta_2(f_{cd}) \ldots \eta_8(f_{cd})]^T$, and $\kappa > 0 \in \mathcal{R}$ is an additional parameter to change the potential field. $\eta(f_{cd_f}) = [\eta_{f1}(f_{cd})\ \eta_{f2}(f_{cd}) \ldots \eta_{f8}(f_{cd})]^T : \mathcal{R}^8 \to [-1, 1]^8$ is defined as in Eq. (30). $f_{x_M}, f_{x_m}, f_{y_M}$ and $f_{y_m} \in \mathcal{R}$ denote the maximum and minimum pixel values along the x- and y-axes, respectively. η and s are functions used to normalize the current pixel value for the maximum and minimum pixel values, and to define the error between the current image features and the final one. The model space navigation function $\tilde{\varphi}(\eta) \in \mathcal{R}^8 \to [0, 1]$ is then defined as

$$\tilde{\varphi}(\eta) := \frac{\varphi}{1 + \bar{\varphi}} \tag{32}$$

The objective function $\bar{\varphi}(\eta) \in \mathcal{R}^8 \to \mathcal{R}$ is defined as

$$\bar{\varphi}(\eta) := \frac{1}{2} s^T(\eta) K_s s(\eta) \tag{33}$$

where $K_s \in \mathcal{R}^{8\times 8}$ is a positive definite symmetric matrix.

The image space navigation function by $\varphi(f_{cd}) \in D \to \mathcal{R}$ can be developed as follows:

$$\varphi(f_{cd}) := \tilde{\varphi} \circ \bar{\varphi} \circ s \circ \eta(f_{cd}) \tag{34}$$

where $\circ$ is the composition operator. The gradient vector $\nabla\varphi(f_{cd})$ can be represented as

$$
\begin{aligned}
\nabla\varphi(f_{cd}) &:= \left(\frac{\partial\varphi}{\partial f_{cd}}\right)^T \\
&= \frac{1}{(1+\bar{\varphi})^2}\mathrm{diag}\left\{\frac{2}{f_{x_M}-f_{x_m}}, \frac{2}{f_{y_M}-f_{y_m}}, \cdots, \frac{2}{f_{y_M}-f_{y_m}}\right\} \\
&\quad\times\mathrm{diag}\left\{\frac{1-\eta_1^{2\kappa-1}\eta_{f1}}{(1-\eta_1^{2\kappa})^{\frac{2\kappa+1}{2\kappa}}}, \cdots, \frac{1-\eta_8^{2\kappa-1}\eta_{f8}}{(1-\eta_8^{2\kappa})^{\frac{2\kappa+1}{2\kappa}}}\right\} K_s s \qquad (35)
\end{aligned}
$$

It should be noted that $f_{cd} \to f_{cd_f}$ from Eqs. (30) to (35) when $\nabla\varphi(f_{cd}) \to 0$.

AUTHORS (from left to right)

  

Toshiyuki Murao received his B.E. degree from the Department of Electrical and Computer Engineering of Kanazawa University in 2003, M.E. degree from the Division of Electronics and Computer Science of Kanazawa University in 2005, and D.Eng. degree from the Department of Mechanical and Control Engineering of Tokyo Institute of Technology in 2008. Since 2006, he has been an assistant professor at the Advanced Institute of Industrial Technology. His research focuses on passivity-based visual feedback control of robot systems.

Hiroyuki Kawai received his B.S. degree from the Department of Electrical and Computer Engineering of Kanazawa University in 1999, and M.S. and Ph.D. degrees from the Graduate School of Natural Science and Technology of Kanazawa University in 2001 and 2004. From 2004 to 2005 he was a postdoctoral scholar at the Information Technology Research Center, Hosei University. In 2005 he joined Kanazawa Institute of Technology as an assistant professor. Since 2010 he has been an associate professor in the Department of Robotics, Kanazawa Institute of Technology. His research focuses on visual feedback control of robot systems and networked cellular vision systems. In particular, he is interested in passivity-based control. He received an IEEE Transactions on Control Systems Technology Outstanding Paper Award from the IEEE Control Systems Society (CSS) in 2008.

Masayuki Fujita is a professor in the Department of Mechanical and Control Engineering of Tokyo Institute of Technology. He is also a program officer of the Japan Science and Technology Agency (JST) Core Research for Evolutional Science and Technology (CREST). He received his D.Eng. degree in electrical engineering from Waseda University in 1987. Prior to his appointment at Tokyo Institute of Technology, he held faculty appointments at Kanazawa University and the Japan Advanced Institute of Science and Technology. His research interests include passivity-based control in robotics and applied robust control. He is currently the CSS Vice President for Conference Activities. He was a member of the CSS Board of Governors. He serves as Head of the SICE Technical Division on Control and previously served as chair of the SICE Technical Committee on Control Theory and as a director of SICE. He served as General Chair of the 2010 IEEE Multi-conference on Systems and Control. His past and present positions include associate editorships of *IEEE Transactions on Automatic Control*, *IEEE Transactions on Control Systems Technology*, *Automatica*, and the *Asian Journal of Control*, and the editorship of the *SICE Journal of Control, Measurement, and System Integration*. He is a recipient of a 2008 IEEE Transactions on Control Systems Technology Outstanding Paper Award. He also received a 2010 SICE Education Award and the Outstanding Paper Award from the SICE.